36

Novoa, E., A. Gonzalez, C. Zambrano, C. Fintina, and O. Gallango, 2003, The petroleum system of the Rubio area, Mérida Andes, Venezuela, *in* C. Bartolini, R. T. Buffler, and J. Blickwede, eds., The Circum-Gulf of Mexico and the Caribbean: Hydrocarbon habitats, basin formation, and plate tectonics: AAPG Memoir 79, p. 797–814.

The Petroleum System of the Rubio Area, Mérida Andes, Venezuela

Enrique Novoa
PDVSA-INTEVEP, Los Teques, Estado Miranda, Venezuela

Angel Gonzalez
Gerencia Exploración, Producción y Mejoramiento, Caracas, Venezuela

Carmen Zambrano
PDVSA-INTEVEP, Los Teques, Estado Miranda, Venezuela

Claudia Fintina
PDVSA-INTEVEP, Los Teques, Estado Miranda, Venezuela

Oswaldo Gallango
PDVSA-INTEVEP, Los Teques, Estado Miranda, Venezuela

ABSTRACT

Integrated studies of the hydrocarbon system in frontier areas are important to assess exploration risk. The Rubio block located in the Táchira Depression has been the focus of various geological studies, yet very few studies of its petroleum system have been published. Based on seismic, surface geologic, and geochemical data, a study of the petroleum system has been developed.

We have identified, based on quality limited seismic and surface data, at least three major periods of deformation in the study area, ranging from the Upper Cretaceous to the present. The first event is of Late Cretaceous age and is characterized by compression. The second period is characterized by extension and took place at least during the Paleocene. Both events may be related to the development of the Colombian Central Cordillera and the flexure caused by its tectonic load, which affected western Venezuela from the Upper Cretaceous to the Paleocene. The third event is characterized by compression that has occurred quite recently, and it may be associated with the development of the Mérida Andes. This last event is responsible for the development of the major structures in the Rubio block. It is worth noting that western Venezuela also was affected by a Jurassic extensional event that is not illuminated by the seismic data of the study area but has been amply shown in both surface and seismic data in the surrounding areas.

According to the 1-D and 2-D geochemical modeling results, we propose that maturity of the source rock (the La Luna Formation) is greater to the west than to the east. Hydrocarbon expulsion from the source rock started in the

western portion of the area 25 m.y. This local kitchen stopped expelling because of its uplift, which was caused by the latest compression. On the other hand, the La Luna Formation in the eastern portion started to expel hydrocarbon very recently, which is still ongoing. This active oil kitchen may be feeding the oil seeps in the eastern part of the study area.

INTRODUCTION

The Rubio area is located in the Táchira Depression, which is a topographic saddle between the Mérida Andes and the Eastern Cordillera of Colombia (Figure 1). The Mérida Andes is a northeast-trending mountain range that extends from the Venezuela-Colombia border in the south to the city of Barquisimeto in the north.

The production of oil in western Venezuela started in this area in 1882. Oil was produced from the Alquitrana seep by a local oil company (León, 1992). In the 1930s and 1940s, oil companies actively explored the area for oil. However, the petroleum system of the area was little known. Recently, PDVSA EP&M has renewed its interest in the Rubio area. Two 2-D seismic reflection data surveys have been shot in the area in the last ten years, but imaging problems did not allow explorers an accurate image of the subsurface structures. Recent reprocessing has improved the quality of the data, making it possible to illuminate the structures and develop balanced cross sections and 1-D and 2-D geochemical models. So far, no well has been drilled in the area.

The objective of this work is to investigate the petroleum system of the study area based on structural analysis and 1-D and 2-D geochemical modeling. The cross sections were developed based on depth-converted time-migrated 2-D seismic profiles and surface data taken from Creole Petroleum Corporation (1957) and Chaplet (1998). Both the cross sections and kinematic model were constructed using fault-bend fold theory (Suppe, 1983).

GEOLOGICAL SETTING

The Rubio area is located close to the zone where interference between the Mérida Andes, Santander Massif, and Colombian Eastern Cordillera occurs (Figure 1). Laubscher (1987) proposed that these are Neogene features and developed as the result of 3-D kinematic interactions between relatively stable blocks in a triple junction formed by the South America, Caribbean, and Nazca Plates. These interactions are accommodated by strike-slip and inverse faults.

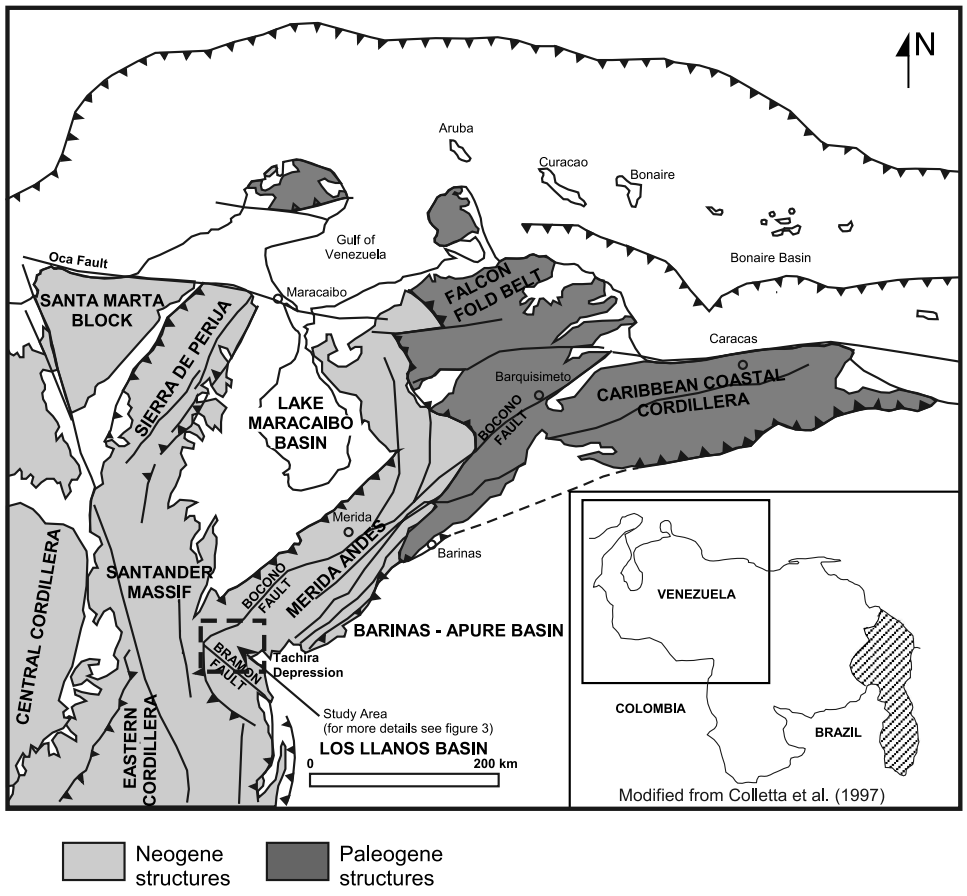

Figure 1. Schematic geologic regional map of eastern Venezuela and western Colombia. Observe that the Rubio area (dashed box) is located where the Mérida Andes, Santander Massif, and Eastern Cordillera interference occurs.

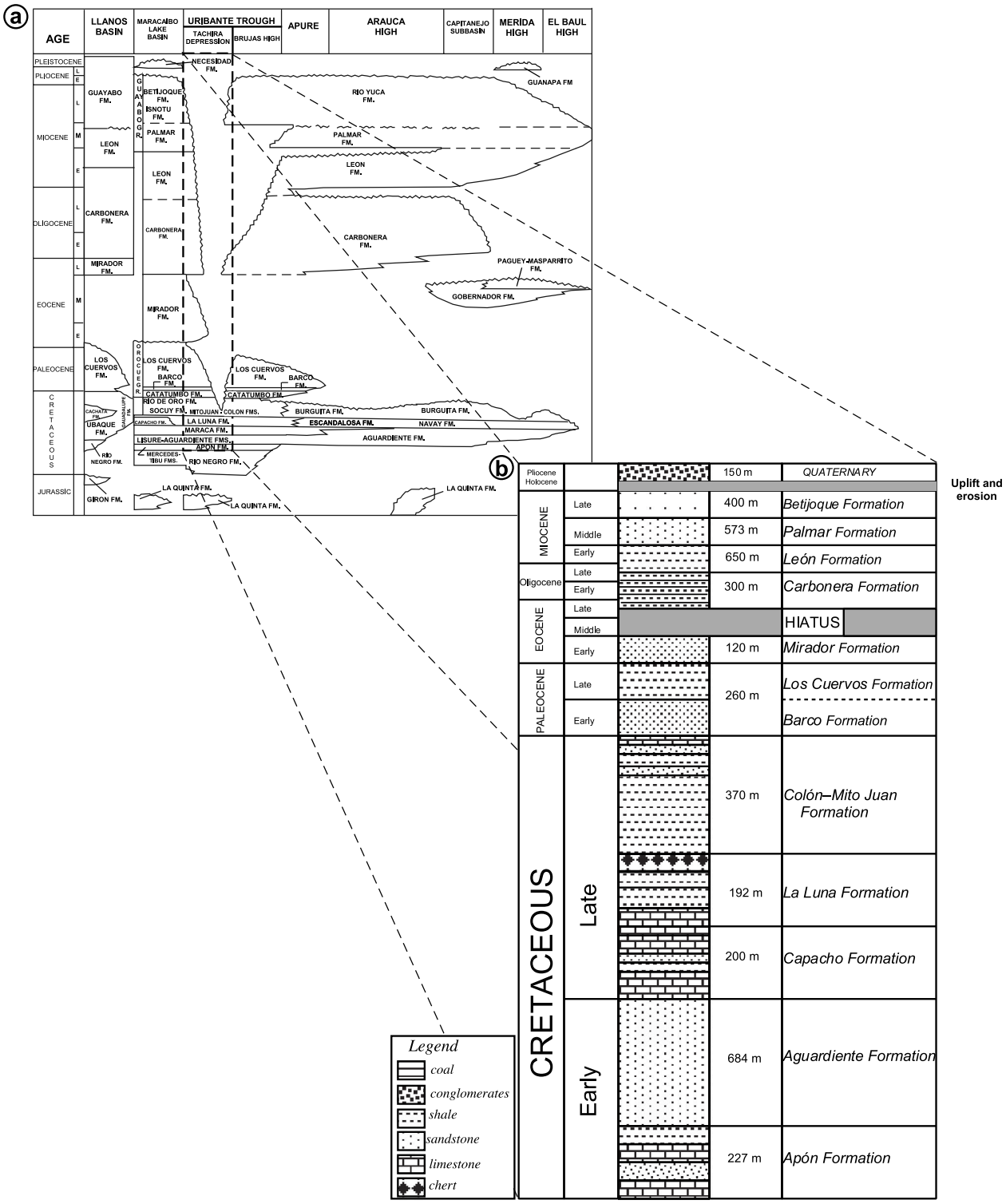

Figure 2. **(a) Stratigraphic chart of Western Venezuela (Código Geológico de Venezuela, 1997). (b) Stratigraphic chart of the study area.**

The magnitude of slip on the major faults in this triple junction (Boconó, Oca, Bucaramanga and other faults) is amply discussed in the literature (e.g., Colleta et al., 1997; Roure et al., 1997; Audemard, 1991; Case et al., 1990; Laubscher, 1987; Maze and Hargraves, 1984; Schubert, 1980; Schubert, 1982; Shagam, 1972; Shagam, 1975).

Figure 2 shows a stratigraphic chart of the western Venezuela basin published by Código Geológico de Venezuela (1997). Parnaud et al. (1995) divided the

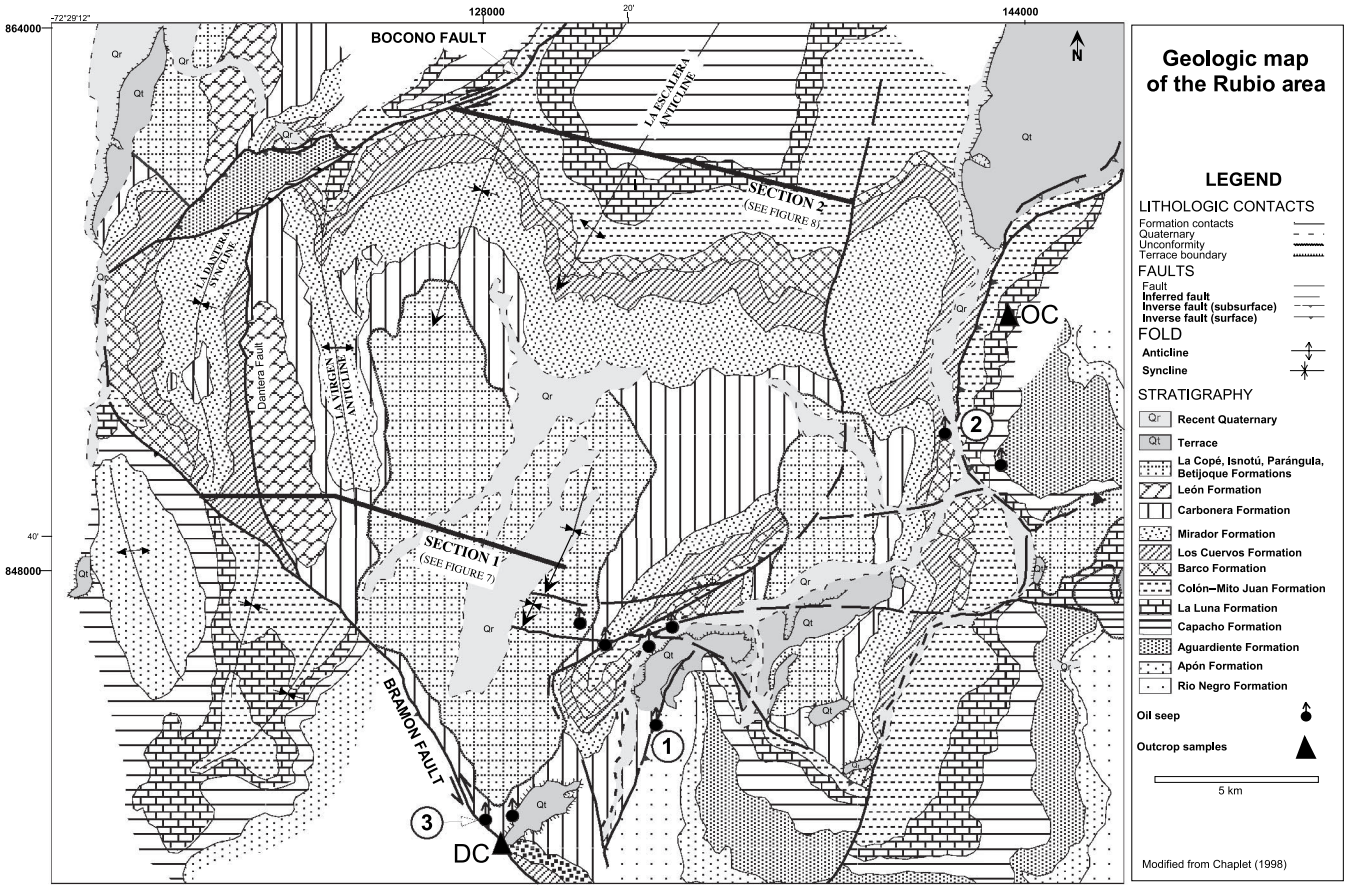

Figure 3. **Detailed geologic map of the Rubio area. Most structures are northeast-southwest oriented. The thicker lines show the location of the balanced cross sections presented in this paper. The outcrops where the La Luna Formation samples were taken to be analyzed are labeled OC and DC (see results in Tables 1, 2, and 3). Sample oil seeps are identified as 1, 2, and 3 (see results in Figure 10 and Table 3).**

Mesozoic-Cenozoic succession of western Venezuela into five sequences based on tectonic events: (1) a Jurassic rift sequence; (2) an Early–Late Cretaceous passive margin sequence; (3) a Late Cretaceous–early Paleocene transitional sequence corresponding to passive margin behind compressive arc; (4) Paleocene–middle Eocene foreland deposits caused by emplacement of the Lara Nappes; and (5) a late Eocene–Pleistocene sequence related to the collision of the Panama arc with the South America Plate. A similar division is presented by Roure et al. (1997).

The Rubio area is bounded to the northwest and southwest by the Boconó and Bramón strike-slip faults, respectively (Figure 3). Meier (1983) and Schwander (1984) have mapped the area and its surroundings in detail. Meier et al. (1987) indicated that this area has structures related to the Venezuelan Andes, Colombian Eastern Cordillera, and the Santander Massif. Their mapping shows that deformation occurs in the brittle domain. This deformation is accommodated by strike-slip, thrust, and reverse faults. They interpret the fold-fault patterns as flower structures. Macellari (1984) interpreted the Rubio block as the decoupling area between the Mérida Andes and the Eastern Cordillera, which is characterized by thrusting. Ostos et al. (1996) indicated that structures in the area are the result of full or partial inversion of Paleozoic crustal-scale discontinuities. They also identify two source rocks for the area: the La Luna Formation of Upper Cretaceous age, and the Los Cuervos Formation of Paleocene age. Their 1-D modeling suggested that oil migration started during the middle Miocene.

GEOMETRY AND KINEMATICS OF STRUCTURES IN THE RUBIO AREA

The structural analysis was divided into two parts: analysis of the combination of axial surface and surface

geology maps (Figures 3, 4, and 5) and development of two balanced cross sections through the area (Figures 6, 7, and 8). This has allowed us to understand the ages of the different structures in the study area and their relationship in map view.

Combination of Axial Surface and Surface Geology Maps

The axial surface map was obtained by using the vertical projection method (Shaw et al. 1994). This method consists of vertically projecting the intersection between axial surfaces and a mapped horizon to a horizontal datum. The intersections between the projected axial surface and the datum are plotted on the map plane. Finally, axial surface maps are generated by linearly connecting the projected points of the same axial surface through the profile grid. This technique helps to define fold trends and lateral changes in structure and to constrain underlying fault geometry and slip. Also, the technique preserves the horizontal position of structures. For this work, the axial surfaces were intersected with the topographic profile and vertically projected onto the shot point map. In order to have a complete picture of the geometry of the different structures in map view, the surface geology map of the study area (Chaplet, 1998) (Figure 3) and the axial surface map were combined (Figures 4 and 5).

A number of axial surfaces have been identified on the map to facilitate the description of the structures in map view: A-A′, B-B′, C-C′, D-D′, E-E′, G-G′, H-H′, I-I′, J-J′, and K-K′ (Figure 4).

Most fold trends (A-A′, B-B′, C-C′, D-D′, E-E′, G-G′, H-H′, and I-I′) show a northeast-southwest orientation parallel to the Mérida Andes. However, the trends J-J′ and K-K′ have an east-west orientation that is nearly perpendicular to the orientation of the other folds (Figures 4 and 5). This causes the development of interference between both groups of fold trends similar to the interference structures reported by Novoa et al. (1998). The fold trends (J-J′ and K-K′)

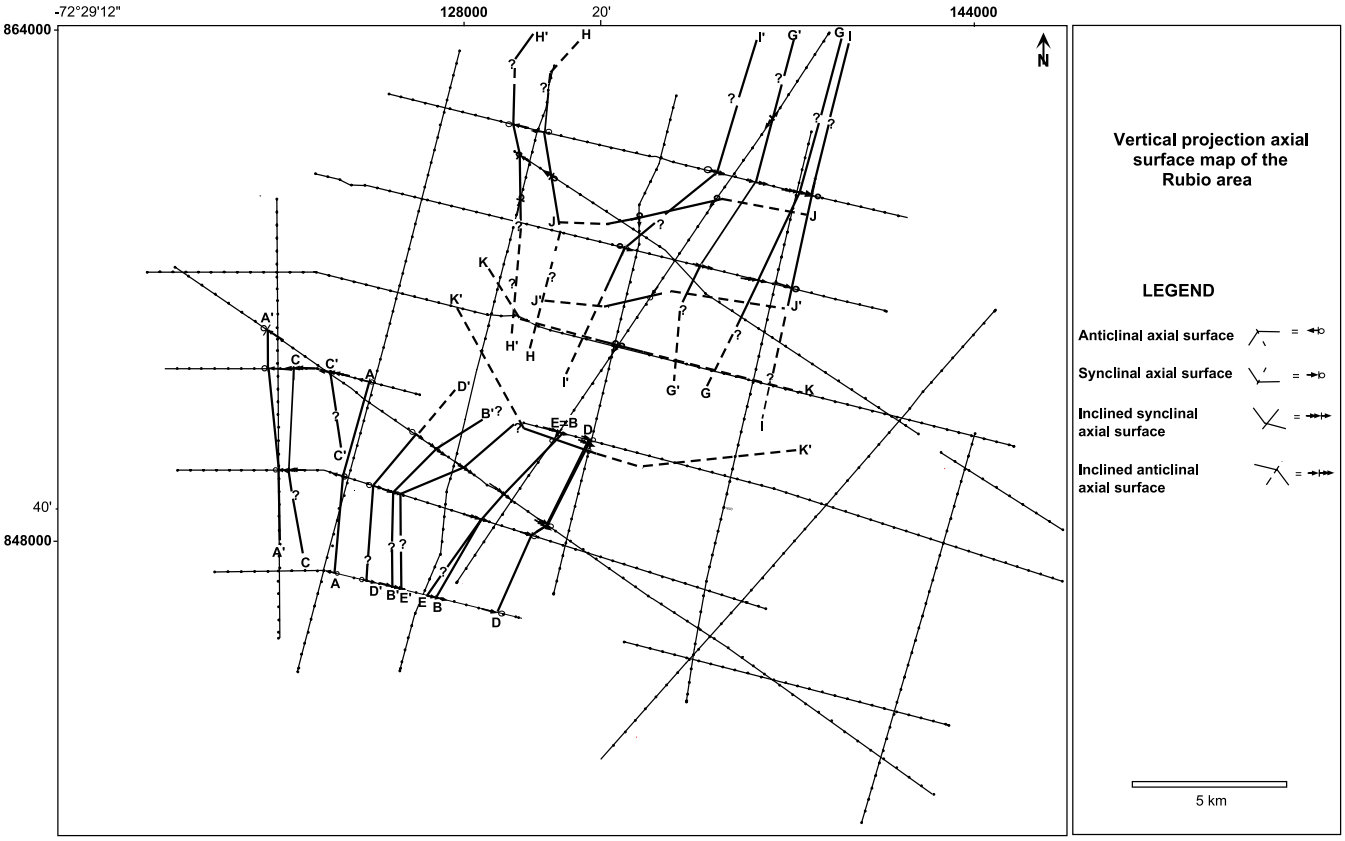

Figure 4. Vertical projection axial surface map developed by using the seismic grid available in the area. Most fold trends have a southwest-northeast strike. In contrast, the fold trends J-J′ and K-K′ have an east-west strike. Both fold-trend families interfere with one other in the center of the study area.

Figure 5. **Combination of the geologic and vertical projection axial surface maps. There is a good correlation between the fold trends mapped from seismic data and those mapped in the geologic map.**

die against a tear fault to the east. On the other hand, both fold trends progressively disappear to the west because of decreasing of their kink-band width. These east-west trending folds may be related to deep lateral ramps.

The kink-band width in map view of the fold trends located to south of the study area (A-A′, B-B′, C-C′, D-D′, E-E′, and F-F′) decreases progressively to the south, probably dying out against the Bramón Fault, and increases to the north (Figures 4 and 5). The axial surface E is offset by a tear fault, which may be caused by a change in the geometry of the related thrust fault.

The kink-band width of the trends G-G′ and H-H′ located in the northern part of the area is interpreted as dying to the south and seems to continue to the north beyond the study area. Meanwhile, the kink-band width of the trend I-I′ increases to the south and decreases to the north. This fold trend continues to the north beyond the mapped area (Figures 4 and 5).

The boundary between the southern and northern fold trends is not defined in either the axial surface map or the surface geology map, but it could represent a tear fault or several tear faults.

BALANCED CROSS SECTIONS THROUGH THE STUDY AREA

Two balanced cross sections were developed using surface geology (Figure 3) and seismic data (Figure 6) to describe the different structures in vertical sections (Figures 7 and 8). Because no well has been drilled in the study area, the formation tops mapped on the geologic map by Chaplet (1998) (Figure 3) were tied carefully to the seismic grid, making it possible to correlate them through the grid. Cross section 1 is located in the southern part of the area (Figures 3 and 7) and cross section 2 is placed in the northern part of the area (Figures 3 and 8).

Figure 7 shows a complex structure that is the result of imbricate thrust faults at different depths.

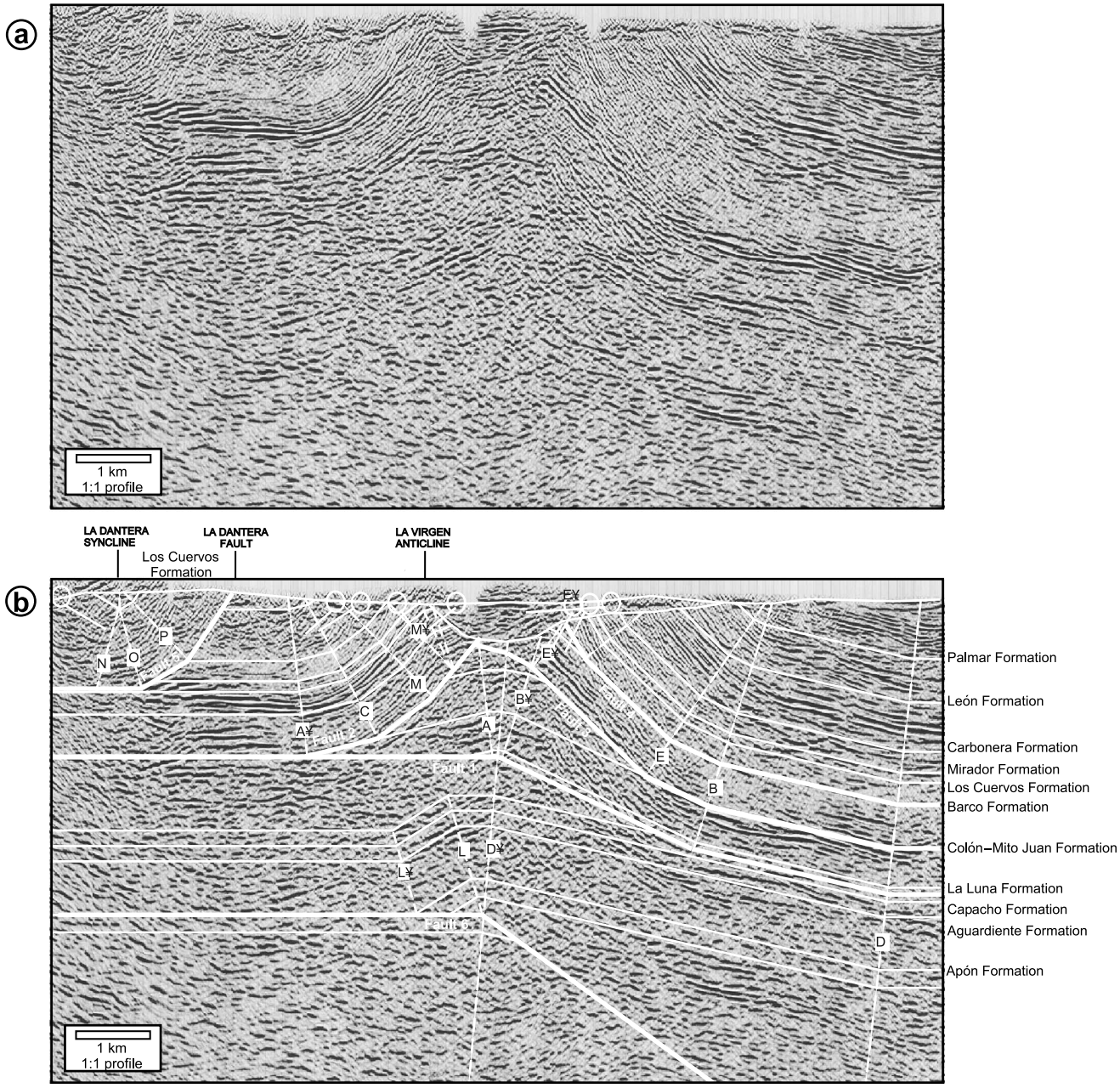

Figure 6. **Depth-converted, time-migrated, 2-D seismic profile of the Rubio area. (a) Uninterpreted. (b) Seismic profile with faults and axial surfaces interpreted. Surface data from Creole map (1957) and Chaplet (1998) were projected on the seismic profile to develop the interpretation.**

Most axial surfaces terminate at shallow faults, but D-D′ and L-L′ terminate at deeper faults. L-L′ is not shown on the axial surface map because it does not extend into the other seismic profiles.

The kink-band D-D′ has been interpreted as the back limb of a fault-bend fold, which develops above a west vergent thrust fault with a cut-off angle of 13°. This fault accommodates 5.2 km of shortening. The depth at which this fault is located cannot be determined. This kink-band folds the shallow and older structures.

The kink-bands B-B′ and A-A′ are interpreted to have developed above the same thrust fault (fault 1). This fault has west vergence, a cut-off angle of 13°, and accommodates 2.4 km of shortening. This fault connects to a back thrust (fault 2), which takes up half of this shortening. As a result of this, the kink-bands C-C′ and M-M′ develop. The back-thrust fault

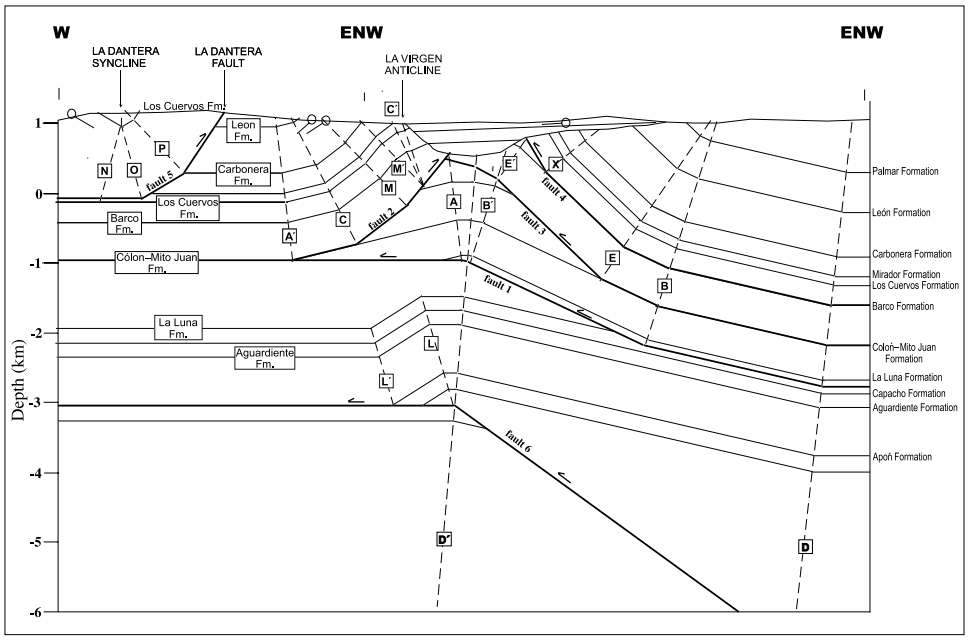

Figure 7. Balanced section 1 (see Figure 3 for location). Most fold trends are related to shallow faults, but kink-band D-D′ may be related to a deep fault.

is decapitated by a Quaternary unconformity. The rest of the shortening is accommodated by a west-vergent décollement in the Colón–Mito Juan Formation shales.

The kink-band E-E′ develops above a west-vergent thrust fault with a cut-off angle of 20° (fault 3). This fault accommodates about 2.0 km of shortening. The synclinal axial surface X is associated with the shallowest thrust fault, which is eroded almost completely. This fault has a west vergence and a cut-off angle of about 14° (fault 4).

The axial surfaces N, O, and P fold the Los Cuervos Formation of Paleocene age and are associated with the north-south-striking fault 5, which is named, at the surface, the La Dantera fault (Figures 3, 6, and 7). The Los Cuervos Formation is thicker to the west of the fault. This observation suggests that this fault grew normally, at least during the Paleocene. This normal fault was inverted in recent times, which put the Los Cuervos Formation in contact with the León Formation of lower Miocene age. Gallango et al. (2002), Fimlay and Gou (1997), and Bueno and Pinto (1997) interpret a similar age for an extensional event in the Perijá fold belt and the Maracaibo Lake basin.

The kink-band L-L′ has been interpreted as having developed above a west-vergent thrust fault with a cut-off angle of 25° (fault 6). This fault accommodates 1 km of shortening and connects to a décollement in the upper shales of the Apón Formation (Figure 2b). However, this structure has been interpreted from poor seismic data (Figure 6). We propose that this structure could have grown after the deposition of the La Luna Formation and during the deposition of the Colón and Mito Juan Formations, locally controlling thickness changes in both formations. Gallango et al. (2002) and Cooney and Lorente (1997) have proposed a similar deformation event in the Perijá Range. This structure was not mapped

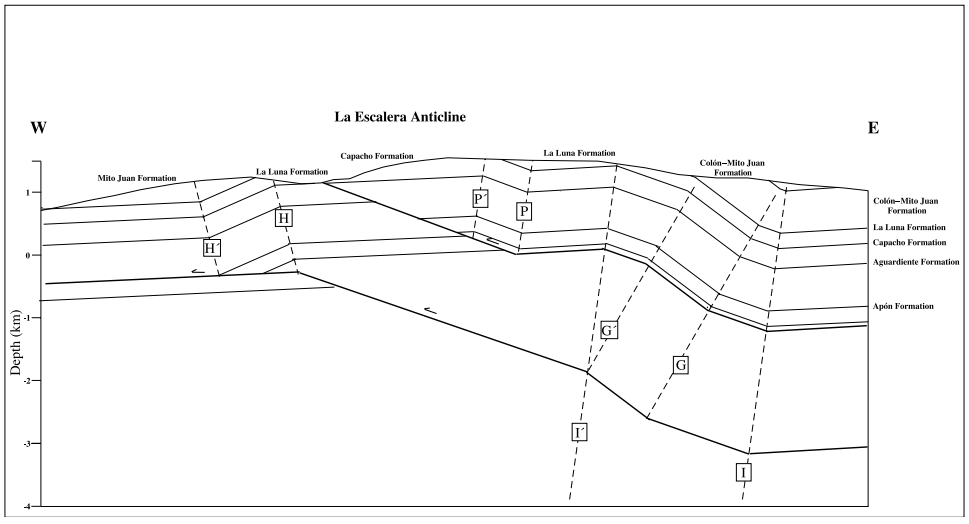

Figure 8. Balanced section 2 (see Figure 3 for location). Similarly to section 1, most fold trends are related to shallow faults. Fold trend I-I′ seems to be related to a deep fault.

on the axial surface map because it is found only along the seismic profile shown in Figure 6. However, we estimate that it should have a northeast-southwest strike. Gallango et al. (2002) show that Upper Cretaceous structures mapped in the Perijá Range have a northeast-southwest strike.

Roure et al. (1997) and Parnaud et al. (1995) showed that western Venezuela was affected by the development of a foreland flexure caused by the emplacement of allochthonous units of the Central Cordillera and Caribbean thrust belts during the Upper Cretaceous to Paleogene. These authors also postulated that these events might be responsible for the regional thickness changes documented in the sequences of this age span. Thus, based on the north-south and northeast-southwest orientation of the La Dantera fault and kink-band L-L′, respectively, the Upper Cretaceous compressional and Paleocene extensional structures documented in the study area could be related to the development of the Colombian Central Cordillera fold belt. Given the data available to do this work, we have not found any evidence of deformation associated with the emplacement of the Caribbean thrust belt in the Rubio area.

Most axial surfaces in section 1 (Figure 7) fold the Betijoque Formation of upper Miocene–Pliocene age; therefore, the structures must have started growing at least since the Pliocene.

Balanced cross section 2 (Figure 8) shows that fold trends (P-P′, G-G′, H-H′, and I-I′) developed above west-vergent shallow and deep-thrust faults. The kink-band P-P′ is related to the shallowest fault, which accommodates about 0.6 km of shortening and dips 22°S. The fold trends G-G′ and H-H′ compose a fault-bend fold that has grown above the same fault. This fault accommodates about 1 km of shortening and dips 19°S. The fold trend I-I′ is related to the deepest fault, which accommodates 3.0 km of shortening and dips 19°S. All these structures may be related to the development of the Mérida Andes.

We have not interpreted any structure below the Apón Formation in both cross sections because of the lack of subsurface data in the study area. However, Parnaud et al. (1995) and Roure et al. (1997) have shown that a Jurassic extensional event affected western Venezuela.

KINEMATIC FORWARD MODEL

In order to generate a 2-D geochemical model, a kinematic model of cross section 1 (Figure 6) was developed using Thrustpack, PDVSA version, and it is shown in Figure 9. Figure 9a presents the initial stage of the model. It shows the future trajectory of fault 6 in undeformed Cretaceous strata. Fault slip causes folding of the hanging wall block along an active axial surface (L) that is pinned to the hanging wall block. The inactive axial surface (L′) is passively translated away from active axial surfaces by slip, thus the flank (L-L′) expands laterally. During this deformation, the Mito Juan and Colón Formations were deposited (Figure 9b). Figure 9c shows the deposition of the Tertiary sequence (from the Barco Formation of Paleocene age to the Betijoque Formation of Miocene-Pliocene age). It also shows the future trajectory of fault 3. In the kinematic model, it has been supposed that fault 3 propagates to the surface (Figure 9d). This causes the development of kink-band E-E′. Additionally, Figure 9d illustrates the future trajectories of faults 1, 2, and 7 (the deepest fault in the section). All these faults propagate until the present configuration is obtained (Figure 9e), in which the western block is uplifted and partially eroded. Faults 4 and 5 have not been modeled. During the kinematic modeling, we have not taken into account the Jurassic extensional event because the geometry of the possible faults and rollovers were not illuminated by the seismic data.

GEOCHEMICAL STUDY

The geochemical study includes source-rock evaluation of outcrop samples, characterization of oil seeps, and 1-D and 2-D geochemical modeling. The main objectives have been the correlation of source rock to oil occurrences, and defining the timing of oil generation and migration.

Source Rock Characteristics

The main source rock in the study area is the highly prolific, oil-prone La Luna Formation, which was deposited under anoxic conditions during the Late Cretaceous (Figure 2). Samples of the La Luna Formation (argillaceous limestone, shale, and limestone) from two outcrops located to the south (DC) and east (OC) of the study area (Figure 3) were analyzed for source-rock evaluation.

The results from Rock-Eval pyrolysis and kerogen microscopy data indicate that in the study area, the La Luna Formation contains good- to excellent-quality

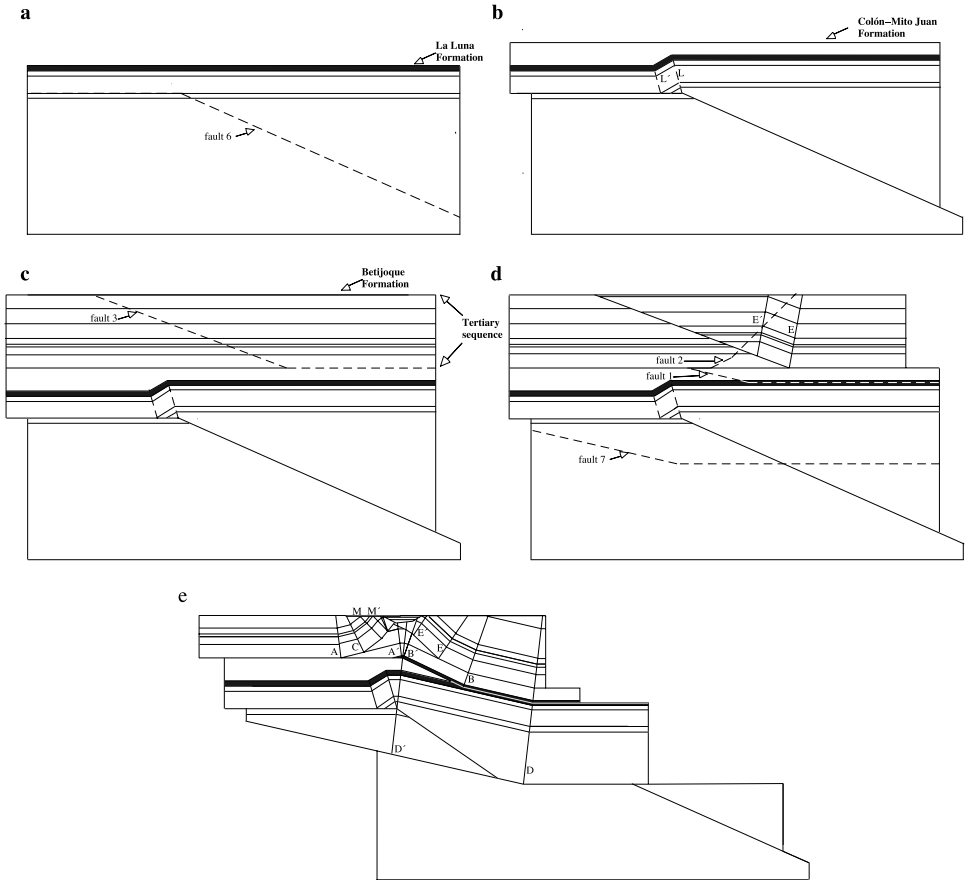

Figure 9. Kinematic model of section 1 developed using fault-bend fold theory (Suppe, 1983). (a) Deposition of the La Luna Formation, showing the future trajectory of fault 6. (b) Propagation of fault 6 and development of kink-band L-L′ and deposition of the Mito Juan Formation. (c) Deposition of the Tertiary sequence, showing the trajectory of fault 3. (d) Propagation of fault 3 and development of kink-band E-E′, showing future trajectories of faults 1, 2, and 7. (e) Present stage; faults 1, 2, and 7 propagate and the structure reaches its present geometry.

type II oil-prone organic matter (essentially unstructured lipid material with minor vitrinite and inertinite). The samples from the OC outcrop show an average TOC of 3.32 and average Ro maturity of 0.67% (Table 1). The La Luna Formation at the DC outcrop contains good to excellent, overmature type II oil-source rock. Samples analyzed from this outcrop show an average TOC value of 2.61% and an average Ro value of 1.72% (Table 2). Comparing the visual kerogen analysis of OC and DC outcrop samples and using the Daly and Edman (1987) method for estimating the original organic carbon (TOC) and hydrogen indices, we determine that the original HI and TOC values at the immature stage probably were ranging between 371 to 865 mgHC/g TOC and 2.62 to 9.30%, respectively. Based on these results, we have used an average of original TOC and HI of 4.94% and 582 mgHC/g TOC, respectively, in the 1-D and 2-D geochemical modeling.

Oil Seeps and Rock Extracts Characteristics

Three oil seeps (labeled as 1, 2, and 3 in Figure 3) and four rock extracts of the La Luna Formation from the OC outcrop were analyzed in order to correlate the oils with the source rock (Figure 10 and Table 3). Both the rock extracts and oil seeps found in the area show very similar biomarker distribution (Figure 10a, b). The terpanes and sterane biomarker data from both the rock extracts and oil seeps indicate marine, algal-bacterial organic matter with negligible terrigenous organic matter. They also show high C_{23} tricyclic/C_{24} tetracyclic terpanes ratios and low to moderate hopane steranes ratio (Hop/St < 3) (Table 3). The elevated amount of C_{27} steranes (37– 42%) (Table 3) suggests a significant contribution to the organic matter from algae. The C_{34} and C_{35} hopanes are well preserved (Figure 10), indicating a reducing, anoxic depositional environment for the source rock. Also, both the rock extracts and oil seeps present a relatively high abundance of gammacerane, having a gammacerane index as high as 0.25 (Table 3), which indicates increasing water salinity during deposition of source rock. On the other hand, in both types of samples, the C_{31} hopanes 20S /(20S + 20R) ratios range between 0.57 and 0.60, and the C_{29} sterane 20S/(20S + 20R)] ratios range between 0.50 and 0.58 (Table 3), indicating similar maturity between the oil seeps and rock extracts.

Table 1. Measurements of total organic carbon (TOC), Rock-Eval pyrolysis, and vitrinite reflectance obtained from the OC outcrop samples of the La Luna Formation. For location of the OC outcrop, see Figure 3.

Depth (m)	*TOC (%)*	*Ro (%)*	*HI (mgHc/gTOC)*	*OI (mg CO_2/gTOC)*
188.6	2.50	0.58	417	14
187.2	3.32	0.51	522	12
186.4	2.40	0.61	542	15
185.5	1.56			
164	2.72		666	9
82.7	3.31		367	11
80.3	3.20		364	11
79.5	2.46		349	12
69.5	1.83	0.78	410	14
65.6	2.67	0.64	378	12
64.6	3.70		326	11
63.5	4.26	0.76	373	8
62.5	3.49		384	8
58	2.01	0.78	495	9
56.8	2.95	0.75	431	11
53.5	2.89		403	6
52	3.20		417	6
51.6	4.31		437	5
50.3	3.97		432	5
49.7	3.08		422	9
49	4.84		374	4
48.6	4.14		440	5
48	4.46		414	7
47.6	3.83	0.76	455	6
47.1	2.25	0.67	438	8
46.7	3.56	0.61	415	6
46.2	3.39		421	6
45.6	4.19		437	5
44.4	3.21		364	25
43.7	4.45	0.65	331	18
41.5	3.90		343	14
38.3	2.07		324	15
36.6	2.61		359	11
35.8	2.08	0.78	335	15
35	2.87	0.72	320	16
33.6	1.86		291	20
29.5	2.18	0.63	303	16
12.2	3.71		350	21
11.6	2.22	0.63	247	27
10.6	2.66	0.66	239	39
10	5.86		347	17
9.5	4.51	0.65	321	19
9	3.91		342	10
8.7	4.22	0.62	381	10
8.1	4.00		390	10
6.7	2.53	0.71	317	18
4.7	2.52	0.55	321	22
2.9	7.47	0.67	354	19

1-D and 2-D Geochemical Modeling

In order to understand the petroleum system in the Rubio area, 1-D and 2-D geochemical models have been developed along section 1 (Figure 11). To perform the 1-D and 2-D geochemical modeling, we have used Basinmod and Thrustpack PDVSA version, respectively. Because the thermal history of

Table 2. Measurements of total organic carbon (TOC), Rock-Eval pyrolysis, and vitrinite reflectance obtained from the DC outcrop samples of the La Luna Formation. For location of the DC outcrop, see Figure 3.

Depth (m)	*TOC (%)*	*Ro (%)*	*HI (mgHc/g.TOC)*	*OI (mg CO_2/g.TOC)*
127.7	1.94		24	50
109	1.86		33	15
107	1.73		45	24
102.7	2.51	1.78	49	14
90.2	2.06		30	9
88	2.27		32	14
79.8	1.58	1.94	35	30
77.4	1.82	1.51	64	20
74.3	1.88	1.50	52	6
70.5	2.14		43	11
70.4	1.52		41	20
69.8	2.76		42	11
69.4	2.46		37	14
68.9	3.30	1.75	47	8
68.3	2.28	1.72	15	64
67.2	2.03	1.71	36	18
66.4	1.97	1.84	27	18
65.1	2.63		59	26
64.7	2.29		26	26
64	3.46		28	29
63	2.63		32	15
62.1	2.36	1.53	14	14
60.2	3.07	1.51	28	28
57.8	3.03		13	63
56.9	3.68	1.72	29	20
56.5	3.64		37	11
48.5	2.32	1.65	18	59
31.1	2.49	1.63	27	62
30.6	3.23		28	18
28.7	4.81	1.77	24	23
28.1	3.52	1.65	38	38
27	2.52	1.85	35	14
26.1	4.08	1.72	34	6
25.1	2.73	1.77	29	22
21.5	2.52	1.82	39	10
20.6	2.41	1.80	33	14
19.8	1.58		49	6
17.8	2.15		10	10
16.2	3.66	1.93	29	14
15.3	3.84	1.73	18	33
14.4	2.33	1.67	29	17
13.4	1.37		24	21

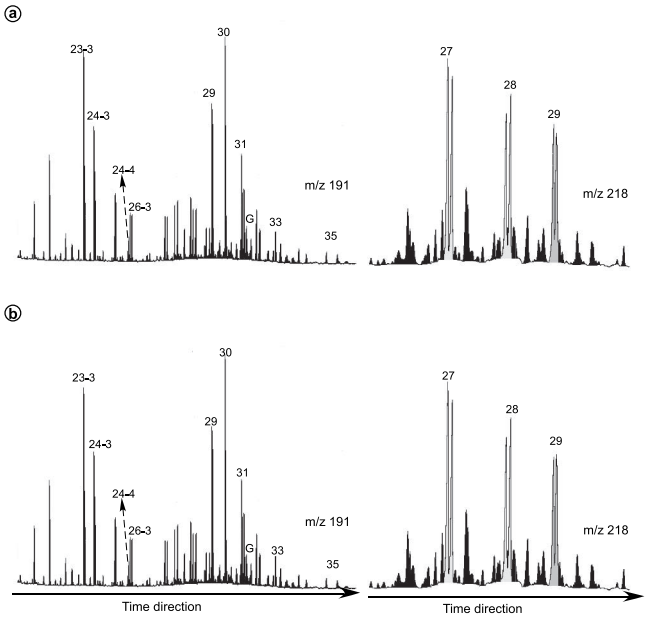

Figure 10. Oil-source rock correlation based on the distribution of terpanes (m/z 191) and steranes (m/z 218). (a) Oil seep 2. (b) Rock extract from the La Luna Formation source-rock in the study area.

the study area is poorly documented, the geochemical modeling was performed with the assumption that the surface temperature has been constant and equal to 25°C; the heat flow has been estimated at 50 mw/m^2, which is equal to the present heat flow in the area. The hydrocarbon generation kinetics determined directly from the La Luna Formation source rock were used during the geochemical modeling. The thermal maturation of the source rock was modeled using default values for basement and radiogenic heat flow included in both software packages. The major uncertainty in our modeling stems from the lack of subsurface data needed for calibration.

Figure 12a and b show the 1-D modeling results of two points (A and B) on section 1 (Figures 11). Point A is located in the western part and point B is located in the eastern part of the section. According to these results, oil expulsion started at point A after the deposition of the León Formation (~ 25 m.y.) and stopped after the uplift of this western block by the deep fault (~ 2.5 m.y.) (Figure 12a). The values of source-rock maturity are predicted to vary between 1.03 and 1.12 %R_o. On the other hand, oil expulsion started ~ 5 m.y. in the east at point B and is still ongoing, as evidenced by lack of significant change in the sedimentary column (Figure 12b). The predicted values of source-rock maturity vary from 0.74 to 1.00. These

Table 3. Biomarker data obtained from the OC outcrop rock extracts of the La Luna Formation and oil seep samples from oil seeps 1, 2, and 3. For locations, see Figure 3.

Type of sample	*Hop/St*	*C_{23} Tricyclic/ C_{24} Tetracyclic*	*C_{35}/C_{34}*	*Gammacerane Index*	*C_{27} (%)*	*C_{28} (%)*	*C_{29} (%)*	*C_{29} sterane 20S/ (20S + 20R)*	*C_{31} hopane 20S/ (20S + 20R)*
Rock extract 1	1.57	0.22	11.7	0.06	40	33	27	0.50	0.57
Rock extract 2	2.11	0.21	9.8	0.19	41	33	26	0.58	0.59
Rock extract 3	2.20	0.31	11.0	0.25	37	37	25	0.56	0.58
Rock extract 4	1.81	0.29	9.9	0.22	42	30	28	0.54	0.59
Oil seep 1	1.65	0.29	9.6	0.25	39	31	30	0.53	0.59
Oil seep 2	1.80	0.27	10.5	0.22	40	30	30	0.55	0.58
Oil seep 3	2.21	0.27	7.4	0.23	41	30	29	0.51	0.60

Gammacerane index = gammacera/(gammacerane+C_{30} hopane).

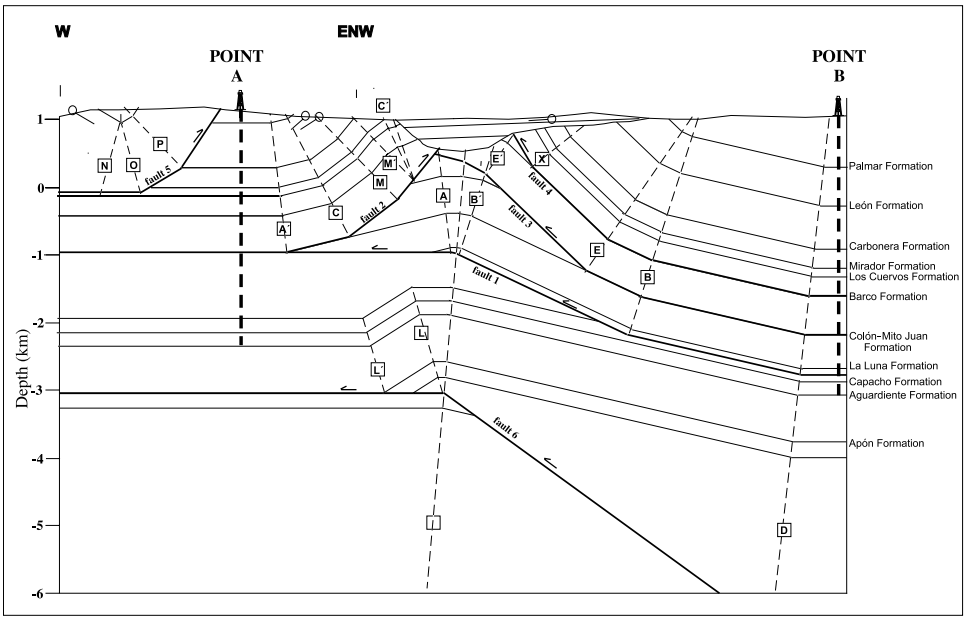

Figure 11. Location of points A and B in section 1, where two 1-D models were developed.

maturity values indicate that the source rock should be expelling oil whose API gravity varies between 25° and 40°. This observation is corroborated by oil seeps located in the area (Figure 3). API gravity measurements in some fresh oil-seep samples show that this oil has a gravity of 30° (Velarde, 1975), and the source rock expelling it should have a maturity (% R_o) equivalent of between 0.74 to 0.85.

Based on the structural geology analysis of the area, a 2-D geochemical model has been developed along section 1 (Figure 7). The 2-D modeling results are shown in Figure 13 and 14. They are very similar to the 1-D modeling results. The vitrinite reflectance (%R_o) of the La Luna Formation is higher in the western portion of the section where the %Ro values vary between 0.90 and 1.30; meanwhile, the %R_o values vary between 0.70 and 1.00 in the eastern portion of the section (Figure 13). This distribution of %Ro is strongly controlled by the thickness change of the Mito Juan–Colón Formations along cross section 1, burying the western portion of the section deeper than the eastern part before the most recent compression (Figure 13d). Afterward, the propagation of the youngest and deepest fault associated in the last 5 m.y., at least, to kink-band D-D′ caused the uplift and erosion of the western portion of the section (Figure 13e).

Similarly to the 1-D modeling results, the 2-D modeling outcome suggests that hydrocarbon expulsion started in the west before the most recent deformation affected the area. The oil expulsion peak from the La Luna Formation in the western side of the section was reached by the end of the deposition of the Betijoque Formation (Figure 14d). At each point in the source rock, the oil expulsion values obtained from the 2-D modeling fluctuate between 150 and 400 bbls/ac-ft. Because the youngest and deepest fault propagates, the western portion of the section is uplifted and partially eroded. Thus, the source rock stops expelling oil. During this deformation event, the La Luna Formation in the eastern part of the section started expelling oil (Figure 14e). The results of the 2-D modeling suggest that oil expulsion values at each point in the source rock in the western part of the section fluctuate between 100 and 400 bbls/ac-ft. Oil expulsion from the La Luna Formation in this side of the section is still active at present.

CONCLUSIONS

The cross sections through the Rubio area show that both low-angle and high-angle reverse faults accommodate shortening. Based on a limited amount of quality seismic and surface data, three periods of deformation have been interpreted in the area: (1) an Upper Cretaceous compressive event, (2) Paleocene normal faulting, and (3) a Pliocene-Pleistocene compressive event. The first two events may be related to the development of the Colombian Central Cordillera.

Most kink-bands are very young, as they fold the Betijoque Formation of upper Miocene-Pliocene age. Thus, they must have developed no earlier than the Pliocene. The kink-band L-L′, interpreted as having developed above a thrust fault, is of Upper Cretaceous age. The La Dantera syncline (axial surfaces N, O, and P) has partially developed above a high-reverse fault, which may be a reactivated normal

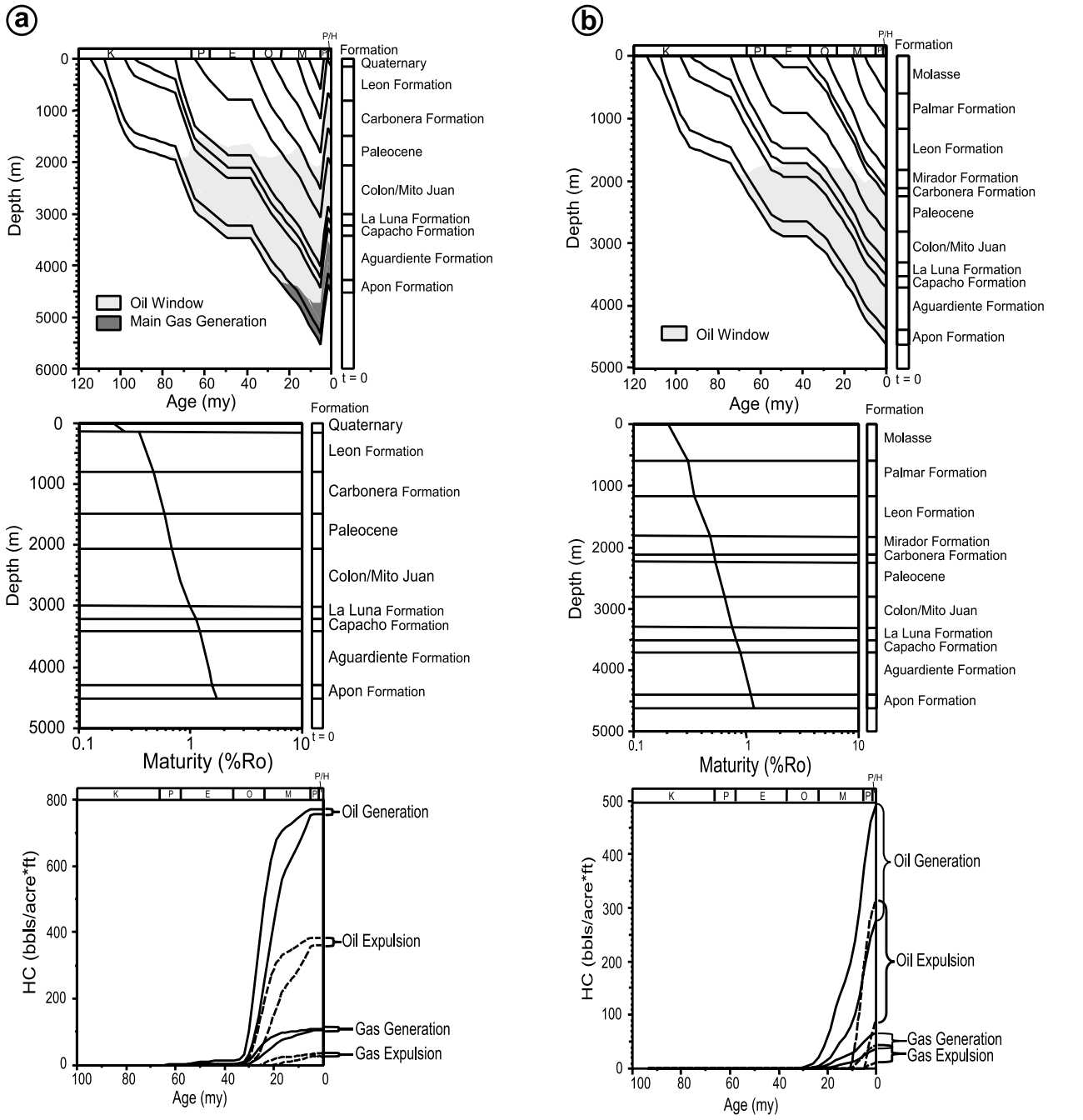

Figure 12. (a) Burial history diagram, modeled maturity, and generation and expulsion (bbls oil and gas per m^3 of source rock) versus time for the La Luna Formation at Point A. (b) Burial history diagram, modeled maturity, and generation and expulsion (bbls oil and gas per m^3 of source rock) versus time for the La Luna Formation at Point B (for location, see Figure 11).

fault. This normal fault could have developed during the Paleocene, as shown by the thickening of the Los Cuervos Formation across the La Dantera fault.

Geochemical modeling suggests that vitrinite reflectance values of the La Luna Formation are greater in the western portion of the area than those in the eastern part. Hydrocarbon expulsion from the La Luna Formation started, first, in the western part of the section before the most recent deformation affected the study area. Once this deformation affected the area, the La Luna Formation in the eastern

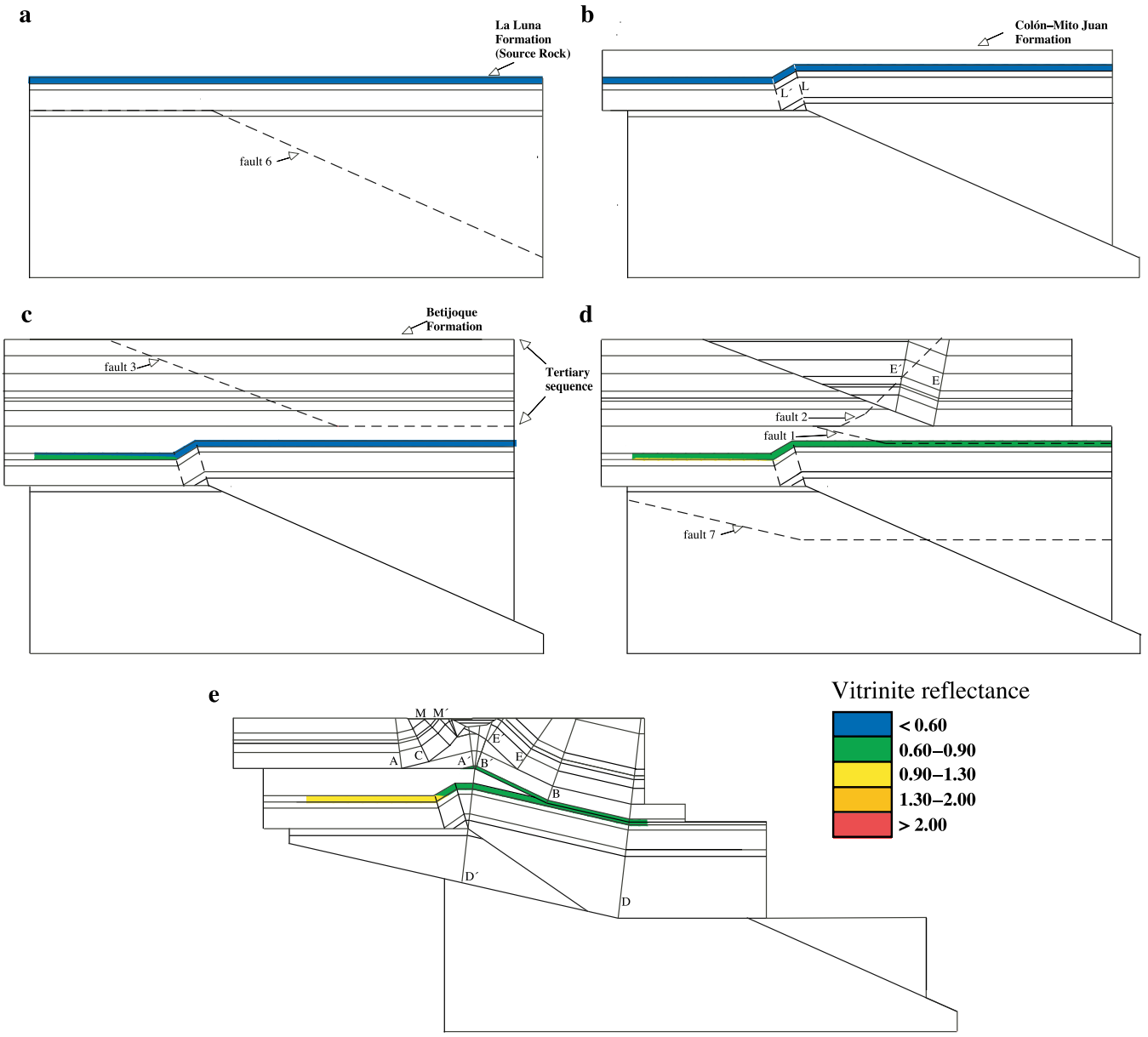

Figure 13. 2-D evolution of the vitrinite reflectance of the La Luna Formation through time. Vitrinite reflectance reaches greater values in the west than in the east. (a, b) Deposition of the La Luna and Colon–Mito Juan Formations do not cause an increment of the vitrinite reflectance values. (c) Deposition of Tertiary sequence produces an increment of the vitrinite reflectance values in the La Luna Formation to the west of the section. (d) The La Luna Formation reaches vitrinite reflectance values of 0.6 to 0.9 along the section. (e) In recent times, the values of vitrinite reflectance are greater (between 0.9 and 1.3) to the west than to the east (between 0.6 and 0.9).

portion stopped expelling hydrocarbons, and the La Luna Formation in the western block started expelling hydrocarbons. This hydrocarbon expulsion is still ongoing and is feeding the oil seeps located to the east of the study area. These results have not been calibrated with subsurface data because the study area has not yet been drilled.

ACKNOWLEDGMENTS

The authors are grateful to PDVSA Exploración, Producción y Mejoramiento and PDVSA-INTEVEP for giving permission to publish this work. This article benefited from constructive suggestions by Dr. A. Pilloud, Dr. F. Roure, and Dr. R. Erlich.

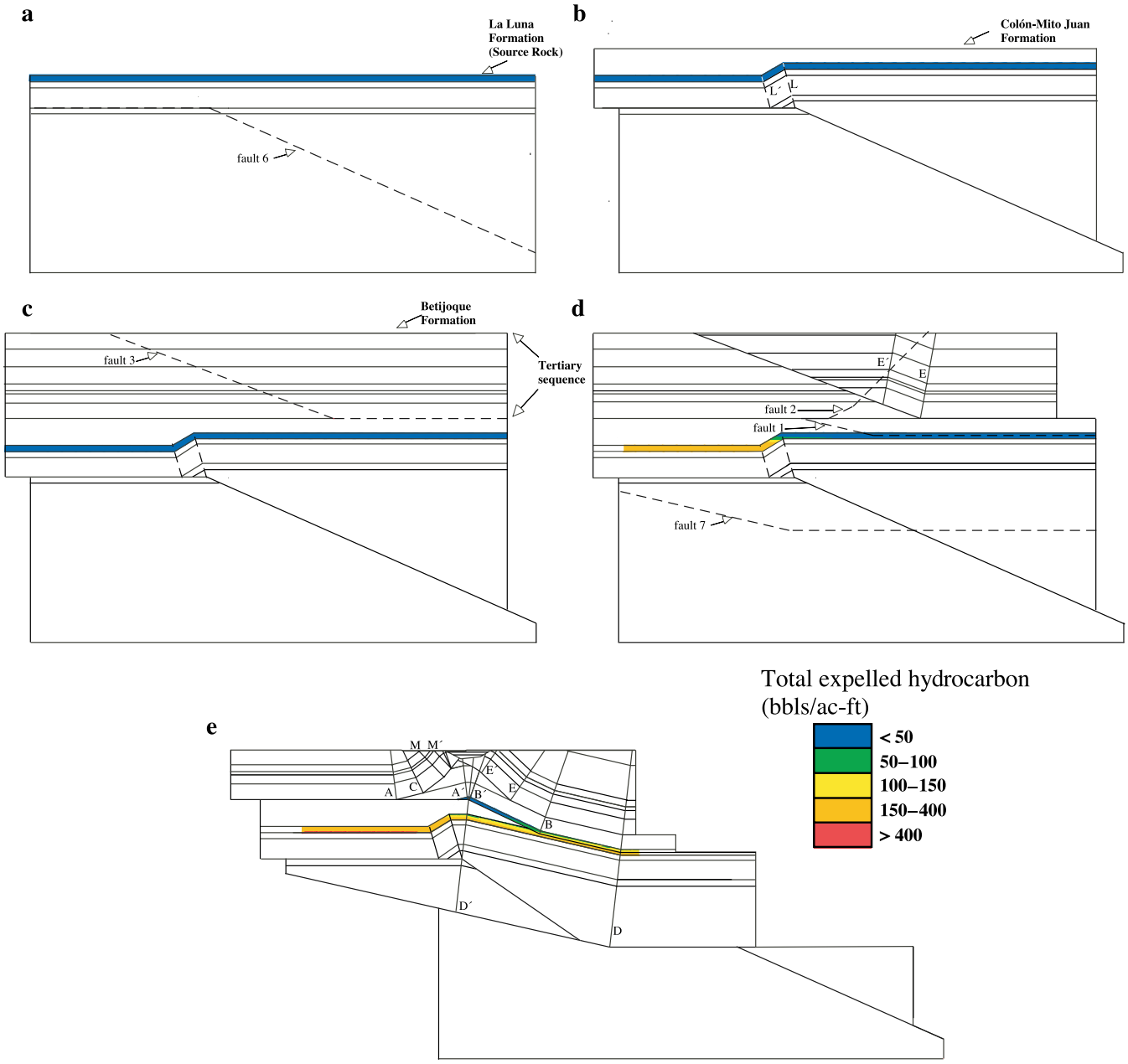

Figure 14. Evolution of the total expelled hydrocarbon from the La Luna Formation through time in the 2-D model. (a, b, c): The deposition of the La Luna, Colon-Mito Juan, and Tertiary Formations do not cause oil expulsion from the source rock. In (d), oil expulsion started first in the western part of the section, reaching its peak during the sedimentation of the Betijoque Formation. In (e), the western part of the section is raised by the propagation of the deepest fault, thus the source rock stops expelling oil. At the same time, oil expulsion from the La Luna Formation starts in the eastern part of the section.

REFERENCES CITED

Audemard, F., 1991, Tectonics of western Venezuela: Ph.D. dissertation, Rice University, Houston, Texas, 245 p.

Bueno, E., and J. Pinto, 1997, Geología Estructural del Alto de Icotea, Lago de Maracaibo: Memorias VIII Congreso Geológico Venezolano, Sociedad Venezolana de Geologia, Caracas, v. I, p. 133–140.

Case, J. E., R. Shagam, and R. F. Giegengack, 1990, Geology of the northern Andes, An overview, *in* G. Dengo and J. E. Case, eds., The Geology of North America, Volume H, The Caribbean Region: The Geological Society of America, p. 177–200.

Chaplet, M., 1998, Mapa geológico de Rubio: PDVSA Exploración, Caracas, Venezuela, Scale 1:100.000.

Código Geológico de Venezuela, 1997, PDVSA-INTEVEP.

[http://www.pdv.com/lexico], [reference: August 28, 2000].

Colleta, B., F. Roure, B. De Toni, D. Loureiro, and H. Passalacqua, 1997, Tectonic inheritance, crustal architecture, and contrasting structural styles in the Venezuela Andes: Tectonics, v. 16, p. 777–794.

Cooney, P., and M. A. Lorente, 1997, Implicaciones tectónicas de un evento estructural en el Cretácico Superior (Santoniense-Campaniense) de Venezuela Occidental: Memorias VIII Congreso Geológico Venezolano, Sociedad Venezolana de Geologia, Caracas, v. I, p. 195-204.

Creole Petroleum Corporation, 1957, Mapa H-2 Geología de Superficie: Creole Petroleum Corporation, Caracas, Venezuela, Scale 1:100.000.

Daly, A. R., and J. D. Edman, 1987, Loss of organic carbon from source rocks during thermal maturation: AAPG Bulletin, v. 71, p. 546.

Fimlay, C., and Y. Gou, 1997, Inversión tectónica de Falla de Pueblo Viejo definida mediante la interpretación de la sísmica 3D en el Campo Bachaquero. Lago de Maracaibo-Venezuela: Memorias VIII Congreso Geológico Venezolano, Sociedad Venezolana de Geologia, Caracas, Venezuela, v. I, p. 267–277.

Gallango, O., E. Novoa, and A. Bernal, 2002, The petroleum system of the Central Perijá fold belt, western Venezuela: AAPG Bulletin, v. 86, p. 1263–1284.

Laubscher, H. P., 1987, The kinematic puzzle of the Neogene Northern Andes, *in* J. P. Schaer and J. Rogers, eds., The Anatomy of Mountain Ranges: Princeton, New Jersey, Princeton University Press, p. 211–227.

León, C., 1992, La Petrolia: El verdadero dorado del Táchira: Boletín de Historia de las Geociencias en Venezuela, v. 45, p. 29–33.

Macellari, C., 1984, Late Tertiary tectonic history of the Táchira Depression, southwestern Venezuelan Andes, *in* W. E. Bonini, R. B. Hargraves, and R. Shagam, eds., The Caribbean–South American plate boundary and regional tectonics: Geological Society of America Memoir 162, p. 333–341.

Maze, W. B., and R. B. Hargraves, 1984, Paleomagnetic results from the Jurassic La Quinta Formation in the Perijá Range and their tectonic significance, *in* W. E. Bonini, R. B. Hargraves, and R. Shagam, eds., The Caribbean–South American Plate Boundary and Regional Tectonics, Geological Society of America Memoir 162, p. 287–293.

Meier, B. P., 1983, Lithostratigraphie und blocktektonik in nödlichen teil der Táchira— Senke (W Venezuela): Ph.D. dissertation, University of Basel, Switzerland, 255 p.

Meier B., M. Schwander, and H. P. Laubscher, 1987, The tectonics of Táchira: A sample of north Andean tectonics, *in* J. P. Schaer and J. Rogers, eds., The Anatomy of Mountain Ranges: Princeton, New Jersey, Princeton University Press, p. 229–237.

Novoa, E., V. Mount, and J. Suppe, 1998, Map-view interference of monoclinal folds: Journal of Structural Geology, v. 20, p. 339–353.

Ostos, M., A. Callejón, S. Talukdar, F. Yoris, R. Lander, M. A. Vivas, J. Oldow, and H. Avé Lallemant, 1996, Petroleum systems of the northwestern Táchira Depression, Venezuelan Andes: II AAPG/Sociedad Venezolana de Geologia International Congress and Exhibition, Caracas, Venezuela, p. A35.

Parnaud, F., Y. Gou, J. C. Pascual, M. A. Capello, I. Truskowski, and H. Passalacqua, 1995, Stratigraphic synthesis of western Venezuela, *in* A. J. Tankard, R. Suarez, and H. J. Welsink, eds., Petroleum basins of South America: AAPG Memoir 62, p. 681–698.

Roure, F., B. Colletta, B. De Toni, D. Loureiro, H. Passalacqua, and Y. Gou, 1997, Within-plate deformations in the Maracaibo and East Zulia basins, Western Venezuela: Marine and Petroleum Geology, v. 42, p. 139–163.

Schubert, C., 1980, Late Cenozoic pull-apart basins, Boconó fault zone, Venezuelan Andes: Journal of Structural Geology, v. 2, p. 463–468.

Schubert, C., 1982, Neotectonics of Boconó fault, western Venezuela: Tectonophysics, v. 85, p. 205–220.

Schwander, M., 1984, Die südliche Táchira-Depression (W Venezuela): Lithostratigraphie, intramiocäne Diskordanz und tektonische Entwicklung im Neogen: Ph.D. dissertation, University of Basel, Switzerland, 242 p.

Shagam, R., 1972, Evolución tectónica de los Andes Venezolanos: Memoria IV Congreso Geológico Venezolano, Caracas, Venezuela, v. 2, p. 1201–1258.

Shagam, R., 1975, The northern termination of the Andes, *in* A. E. M. Nairn and F. G. Stehli, eds., The Ocean Basins and Their Margins, v. 3, The Gulf of Mexico and the Caribbean: New York, Plenum, p. 325–340.

Shaw, J. H., S. C. Hook, and J. Suppe, 1994, Structural trend analysis by axial surface mapping: AAPG Bulletin, v. 78, p. 700–721.

Suppe, J., 1983, Geometry and kinematics of fault-bend folding: American Journal of Science, v. 283, p. 684–721.

Velarde, H., 1975, Importancia de la exploración petrolera y valor comercial de las acumulaciones petrolíferas de la región de Alquitrana, Edo. Táchira: Ediciones Petroleos de Venezuela, Maracaibo, 49 p.